Available online at www.sciencedirect.com
SCIENCE DIRECT®
Optics Communications 250 (2005) 389–397
OPTICS COMMUNICATIONS
www.elsevier.com/locate/optcom

Optical simulation of vertical-cavity surface-emitting lasers with non-cylindrical oxide confinement

P. Nyakas [a,*], Zs. Puskás [b], T. Kárpáti [c], T. Veszprémi [c], Gy. Zsombok [c], G. Varga [a], N. Hashizume [b]

[a] Institute of Physics, Budapest University of Technology and Economics, H-1111, Budafoki út 8, Budapest, Hungary
[b] Furukawa Electric Institute of Technology Ltd., H-1158 Késmárk u. 24-28, Budapest, Hungary
[c] Department of Inorganic Chemistry, Budapest University of Technology and Economics, H-1521, Gellért tér 4, Budapest, Hungary

Received 14 October 2004; received in revised form 1 February 2005; accepted 14 February 2005

Abstract

Two extensions of weighted index method are presented in order to calculate the splitting of degeneracy for non-circular vertical-cavity surface-emitting lasers. Both of them automatically satisfy which transverse optical modes split, and give a reliable approximation for the resonant frequencies, threshold gains and confinement factors. The intuitive effective radius method traces back the splitting for different effective aperture radii which are defined according to the transverse intensity distributions. The hybrid analytical axial and numerical lateral method is more precise from a _mathematical point of view, and provides the mode patterns as well as the optical data.

PACS: 42.55.P; 42.60.D

Keywords: Vertical-cavity surface-emitting lasers; Non-circular oxide aperture; Optical simulations; Weighted index method; Finite difference methods

1. Introduction

Vertical-cavity surface-emitting lasers (VCSELs) have shown promise in telecommunication applications due to their particular properties. They have good optical beam quality, excellent coupling efficiency into optical fibers, are suited for high-speed modulation and for cost-effective mass production. A further advantage is that they have the possibility to be integrated into 2-D arrays. The performance of VCSELs has improved significantly through the use of oxide or air apertures [1,2], which provide

* Corresponding author. Tel.: +361 463 4193; fax: +361 463 4357.
E-mail address: pnyakas@wigner.bme.hu (P. Nyakas).

0030-4018/$ - see front matter © 2005 Elsevier B.V. All rights reserved.
doi:10.1016/j.optcom.2005.02.034

transverse confinement for the injected carriers as well as for the optical field.

One goal of VCSEL-design is to reduce the threshold current. In relatively large devices it is proportional to the volume of the electrically pumped active region, so that smaller apertures are required. As a consequence of good transverse optical confinement VCSELs usually support several transverse modes, and their intensity is determined by the strongly coupled electronical–optical system. The complicated mode behavior seems to be typical for VCSELs with oxide apertures. Considerable work has been carried out to identify mechanisms that determine the transverse mode formation: interaction of cavity structure and gain medium [3], induced birefringence [4,5] and non-circular oxide-windows [6] have been found to play important roles for VCSEL's emission.

In this work, we focus only on the optical mode simulation resulting in the resonant frequencies, threshold gains and optical mode patterns. Several models with different approximations and computation efforts have been presented in this field [7]. The effective index method (EIM) [8,9] replaces the axial structure of the diode with effective indices for the core and cladding(s), and gives an analytical solution similar to the circular optical waveguides for the radial intensity distribution. The weighted index method (WIM) [10,11] takes the radial distribution into account for re-calculating the axial problem, and the final solution is got by an iteration between the two directions. Both methods have been applied only for circularly symmetric VCSELs. They neglect diffraction and scattering losses, which have to be calculated separately [12,13] in order to give a corrected value for the threshold gain. 3-D finite element method (FEM) [14,15] is a numerical solution of the open cavity eigenvalue problem, where assuming circular symmetry decreases the computation domain and simulation time. This numerical technique is, however, always slower than analytical methods by few order of magnitudes.

It may occur that the oxide aperture was not ideally circular due to manufacturing reasons. If oxidation speed were ideally isotropic, the aperture shape would be the exact replica of the mesa geometry. Some groups have already reported that oxidation speed in [1 0 0] direction is higher compared to that of [1 1 0] direction [16,17], and the final aperture may differ from the transverse mesa shape. The violation of cylindrical symmetry can remove the degeneracy of the eigenmodes and modify the important optical parameters and also the mode patterns.

We present two models in this article that describe both qualitatively and quantitatively the effects of non-circularity, and do not demand large computational resources. They fit the hierarchical modeling concept as they improve from semi-analytical to numerical methods, and simultaneously increase from 1 + 1 dimensional modeling (WIM) to 1 + 2 dimensions. A group theoretical introduction is given first, which is used to predict the mode splitting. Effective radius-weighted index method (ER-WIM) is presented next to obtain a simple quantitative analysis of the effect of non-circular apertures. Hybrid WIM provides a deeper mathematical description of the resonant cavity. Finally, we compare the calculated optical data to measurements and conclude.

2. Theory

2.1. Group theoretical considerations

As the modes of the electromagnetic field follow the symmetry of the laser diode, they should follow the transformational properties of the respective symmetry group. Accordingly, as a VCSEL of cylindrical symmetry belongs to the $C_{\infty v}$ symmetry group, each optical mode of the diode has the same transformational characteristics as one of the irreducible representations of the group.[1] In Table 1, a part of the character table of the $C_{\infty v}$ group can be seen together with the shape of the first few LP modes. Only the LP_{0v} modes belong to the non-degenerated A_1 irreducible representation, all the others are doubly degenerated as they belong to any of the E representations.

[1] Here and below, we follow the Schönflies notation (see, e.g. [18]). This labelling system is generally used in spectroscopy and for the description of molecular symmetry.

Table 1
The $C_{\infty v}$ point group and LP-modes

$C_{\infty v}$	I	$2C_{\infty}^{\varphi}$	Pattern	Symbol
A_1	1	1		LP_{01}
A_2	1	1		
E_1	2	$2\cos(\varphi)$		LP_{11}
E_2	2	$2\cos(2\varphi)$		LP_{21}
E_3	2	$2\cos(3\varphi)$		LP_{31}
E_4	2	$2\cos(4\varphi)$		LP_{41}

If the shape of the aperture is distorted, it breaks the cylindrical $C_{\infty v}$ symmetry of the diode and the optical modes follow the transformational properties of the new group. The correlation of the old and the possible new groups can be seen in Table 2. For the sake of compatibility, A, B and E symbols are applied for the irreducible representations of the $C_{\infty v}$ point group. If, for example, the aperture has a square shape, the diode symmetry is C_{4v} and every second, originally degenerated (E-species) pair of modes should split and form individual non-degenerated A_1 and A_2, or B_1 and B_2 modes. If the square shape breaks further (e.g., rectangular or ellipse shape), the new C_{2v} symmetry group prohibits any degeneracy. On the basis of this simple consideration we can easily estimate the degeneracy or non-degeneracy of a given mode.

2.2. Effective radius-weighted index method

The shape of the oxide aperture investigated in this article is a curvilinear tetragon, as realistic apertures usually have two perpendicular symmetry axes and four edges, and are round elsewhere. A good example illustrating the corners and their possible effects on reliability issues can be found in [19]. From simulation aspects a formula is needed that approximates this shape. Debernardi et al. [20] suggested to describe a general aperture with the following Fourier-series:

$$r(\varphi) = r_0\left[1 + \sum_k \Delta_{2k}\cos(2k\varphi)\right], \tag{1}$$

where r_0 is the original (averaged) radius, the Δ_{2k} values denote the coefficients. Δ_4 controls the square-like shape. Using appropriate values for the Δ_{2k} parameters a wide spectrum of aperture shapes can be approximated (see Fig. 1(a)). This formula allows, however, only round shapes, and together with ER-WIM may lead to unwanted degeneracies as discussed in details at the end of this section. The following formula has been found to fit better to the experimental shape (see Fig. 1(b)):

$$r(\varphi) = cr_0 + (1-c)r_{sq}(\varphi), \tag{2}$$

where $r_{sq}(\varphi)$ describes a square in polar coordinate system. With the help of the c "cylindricity" parameter the circle–square transition can be

Table 2
Correlation between $C_{\infty v}$, C_{4v} and C_{2v} symmetry groups

$C_{\infty v}$	C_{4v}	C_{2v}
A_1	A_1	A_1
A_2	A_2	A_2
E_1	E_1	$B_1 + B_2$
E_2	$B_1 + B_2$	$A_1 + A_2$
E_3	E_3	$B_1 + B_2$
E_4	$A_1 + A_2$	$A_1 + A_2$

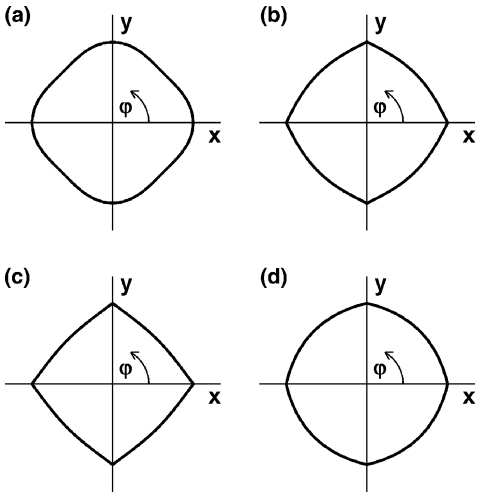

Fig. 1. Aperture models: (a) shows the shape defined by Eq. (1) with $\Delta_2 = 0$ and $\Delta_4 = 1/16$. Curves (b)–(d) are given by Eq. (2) with $c = 0.5$, 0.25 and 0.75, respectively.

scaled. The realistic experimental oxide shape is closest to the one halfway between the ideal circular and square cases (Fig. 1(b)). Fig. 1(c) and (d) display model apertures for comparison with cylindricity parameter of 0.25 and 0.75, respectively.

The model aperture belongs to the C_{4v} symmetry group, as it still has two symmetry axes and shows a rotational symmetry of 90°. As a consequence of Table 2, for odd μ values the degeneracy of the $LP_{\mu\nu}$ modes remains, while for even ones does not. Since degenerated modes have the same optical properties they can be observed together, and the sum of their intensity distribution forms distorted rings.

Apertures of general shape can be approximated with cylindrical apertures of proper radius from certain point of view. Noble et al. [21] used a circular aperture having the same area instead of the assumed square aperture ($r = a/\sqrt{\pi}$) to compute the optical parameters of the fundamental mode. The simple condition for the areas does not answer the degeneracy splitting. By defining different effective radii for the splitted transverse modes and executing two WIM-iterations the effect could be reproduced. Therefore we define the effective radii as a weighted integral of the $r(\varphi)$ function describing the shape

$$R_{1,2} = \frac{\int_0^{2\pi} r(\varphi) g_{1,2}(\varphi)\, \mathrm{d}\varphi}{\int_0^{2\pi} g_{1,2}(\varphi)\, \mathrm{d}\varphi}. \tag{3}$$

Here, $g_{1,2}(\varphi)$ denotes the weighting factors of the two modes, respectively. They must be chosen such a way that the two effective radii should differ in the case of degeneracy splitting (for even μ values), and are equal if degeneracy remains (for odd μ values). The optical parameters calculated from these radii should also match the experimental data. The right choice for the weighting functions can be the intensity distributions because they intrinsically reflect the existing or non-existing degeneracies. Assuming that the aperture only slightly deviates from the circle, the φ-dependencies of the known intensity patterns of the circular structure were used:

$$g_{1,2}(\varphi) = \begin{pmatrix} \sin^2(\mu\varphi) \\ \cos^2(\mu\varphi) \end{pmatrix}. \tag{4}$$

This formula gives one effective radius for $\mu = 0$. With the aperture shape of (1) produces the same radii for odd μ values according to the previous expectation. If the last non-zero coefficient in the Fourier-series is Δ_{2K}, it provides two different radii only if $\mu \leqslant K$ even. This means that in order to predict correctly the degeneracy splitting of higher order modes further coefficients must be defined when using (1). This problem does not occur when using the shape function (2).

2.3. Hybrid weighted index method

In this chapter, a simple scalar formulation of WIM is presented for general non-circular apertures. It predicts correctly the splitting of degeneracy due to the distortion of the rotational symmetry, but does not take polarization into account. An improved vectorial version of this method is also feasible, but demands a more difficult handling of the boundary conditions (in which the electric and magnetic field components are coupled) at the core-cladding interface. Let us write one dominant transverse field component in the form of $E(x,y,z,t) = E(x,y,z)\mathrm{e}^{\mathrm{i}\omega t}$. The field must satisfy the Helmholtz-equation

$$\left[\Delta + \varepsilon(x,y,z)\frac{\omega^2}{c^2}\right] E(x,y,z) = 0, \tag{5}$$

where ε is the piecewise constant dielectric function. In general cases $E(x,y,z)$ is not separable because of the diffraction at the oxide aperture. By neglecting this effect the following separation is made in the longitudinal and the lateral components, but no harmonical dependence is assumed in the azimuthal angle: $E(x,y,z) = P(x,y)Q(z)$. Inserting this ansatz into Eq. (5)

$$\frac{\partial^2 Q(z)}{\partial z^2} P(x,y) + \Delta_T P(x,y) Q(z) + \varepsilon(x,y,z)\frac{\omega^2}{c^2} P(x,y) Q(z) = 0, \tag{6}$$

where $\Delta_T = \partial^2/\partial x^2 + \partial^2/\partial y^2$ is the transverse Laplace-operator. By multiplying with $Q^*(z)$ and integrating against z from the lower to the upper boundary planes of the VCSEL, and multiplying with $P^*(x,y)$ and integrating for the

xy-cross-section of the diode, the original partial differential equation splits into two coupled equations:

$$\left[\left\langle Q\left|\frac{\partial^2 Q}{\partial z^2}\right\rangle + \frac{\omega^2}{c^2}\langle Q|\varepsilon|Q\rangle_{(x,y)}\right]P(x,y) + \langle Q|Q\rangle \Delta_T P(x,y) = 0, \tag{7}$$

$$\left[\langle P|\Delta_T P\rangle + \frac{\omega^2}{c^2}\langle P|\varepsilon|P\rangle_{(z)}\right]Q(z) + \langle P|P\rangle\frac{\partial^2 Q(z)}{\partial z^2} = 0. \tag{8}$$

In order to make the following derivations simpler, P and Q are assumed to be normalized. The coordinates in the lower indices in the above expressions show that the weighted dielectric constant may depend on the coordinates omitted from the integration. For piecewise constant dielectric functions $\langle P|\varepsilon|P\rangle_{(z)}$ is a step-like function of the z-coordinate, and its values can be denoted as $\langle\varepsilon\rangle_j^P$, where j refers to the jth layer ($j = 1$ denotes the substrate, $j = N$ is air). The same way $\langle Q|\varepsilon|Q\rangle_{(x,y)}$ can be reduced to $\langle\varepsilon\rangle_i^Q$, where $i = 1$ for the core region and $i = 2,3,\ldots,M$ for the cladding(s). Eq. (8) is a second-order ordinary differential equation in the jth layer, and the general analytical solution reads as follows:

$$Q_j(z) = a_j e^{i\beta_j z} + b_j e^{-i\beta_j z} \tag{9}$$

and

$$\beta_j^2 = \langle P|\Delta_T P\rangle + \frac{\omega^2}{c^2}\langle\varepsilon\rangle_j^P \quad (j = 1,\ldots,N) \tag{10}$$

is the propagation constant. $Q(z)$ and $\partial Q(z)/\partial z$ must be continuous at each interface between the layers, and only outgoing waves are allowed out of the structure. This problem is solved by the transfer matrix method and a root finding routine on the complex frequency-plane. Knowing the general solution for $Q(z)$ we define k_i^2 as

$$\begin{aligned} k_i^2 &= \frac{\omega^2}{c^2}\langle\varepsilon\rangle_i^Q + \left\langle Q\left|\frac{\partial^2 Q}{\partial z^2}\right\rangle\right. \\ &= \frac{\omega^2}{c^2}\langle\varepsilon\rangle_i^Q - \left\langle Q\left|\beta_j^2\right|Q\right\rangle \\ &= \frac{\omega^2}{c^2}\langle\varepsilon\rangle_i^Q - \langle\beta^2\rangle^Q \quad (i = 1,\ldots,M). \end{aligned} \tag{11}$$

Eq. (7) can be rewritten, and it is clear that k_i plays the role of the lateral propagation constant

$$k_i^2 P(x,y) + \Delta_T P(x,y) = 0 \quad (i = 1,\ldots,M). \tag{12}$$

Before describing in detail how to solve the lateral problem, we point out the iterational procedure between the longitudinal and lateral dimensions. Multiplying Eq. (12) with $P^*(x,y)$, and integrating over the whole cross-section of the diode

$$\sum_{i=1}^{M}\int_{A_i} P^*(x,y)k_i^2 P(x,y)\,dx\,dy + \langle P|\Delta_T P\rangle = 0, \tag{13}$$

where A_i refers the ith region. The sum gives the weighted lateral propagation constant $\langle k^2\rangle^P$. Inserting it into Eq. (10) the same expression is got for β_j^2 as Eq. (11)

$$\beta_j^2 = \frac{\omega^2}{c^2}\langle\varepsilon\rangle_j^P - \langle k^2\rangle^P. \tag{14}$$

The order of the iteration is the following. At first step the axial part is solved assuming $\langle k^2\rangle^P = 0$. The weighted axial propagation constant $\langle\beta^2\rangle^Q$ is calculated next. Substituting it into Eq. (11) the lateral problem is computed. With the lateral propagation constant Eq. (14) is used to refine the axial solution, etc. The iteration stops if the difference for both the real and imaginary parts of the frequency were lower in a cycle than a previously defined threshold.

Now we move on the solution of Eq. (12) in case of non-circular apertures. While for special cylindrical structures analytical solutions are known: the Bessel-functions, here only numerical methods are applicable. Finite difference method (FDM) has been chosen on a non-equidistant rectangular grid. Since the problem is an eigenvalue equation for the complex frequencies as eigenvalues and for the field distributions as eigenvectors, a system matrix containing only the inner nodes of the core and cladding(s) is wanted. The nodes at the interfaces must be expressed using the boundary conditions and eliminated from the unknown variables, and simultaneously the fields at the surface were taken equal to zero. In order to give an elegant solution, an algebraic matrix-description of the following differential equation is presented:

$$\left(\frac{\omega^2}{c^2}\langle\varepsilon\rangle_i^Q - \left\langle\beta^2\right\rangle^Q\right)P(x,y) + \Delta_T P(x,y) = 0. \quad (15)$$

Let us denote the discretized values of $P(x,y)$ as $\bar{P}$. The discretized difference equation has the form of

$$\left(\frac{\omega^2}{c^2}\bar{\bar{\varepsilon}} - \left\langle\beta^2\right\rangle\bar{\bar{I}}\right)\bar{P} + \bar{\bar{\Delta}}\bar{P} = \bar{0}, \quad (16)$$

where $\bar{\bar{\varepsilon}}$ denotes the diagonal matrix of the dielectric constant, $\bar{\bar{I}}$ the identity matrix and $\bar{\bar{\Delta}}$ the sparse matrix of the transverse Laplace-operator. Rearranging the equation one gets

$$\frac{\omega^2}{c^2}\bar{\bar{\varepsilon}}\bar{P} = \left(\left\langle\beta^2\right\rangle\bar{\bar{I}} - \bar{\bar{\Delta}}\right)\bar{P}, \quad (17)$$

which is a generalized algebraic eigenvalue problem, and can be solved using standard routines. Finally, the propagation constants were expressed using Eq. (11). It is important to note that the transverse confinement factor is simply $\int_{\text{core}} P^*(x,y)P(x,y)\,\mathrm{d}x\,\mathrm{d}y$, the intensity in the core.

3. Results

The effective radius-WIM and the hybrid WIM techniques were tested on a GaAs/AlGaAs multimode VCSEL designed for 850 nm emission. It consists of a λ-length cavity and 18 pair top- and 25 pair bottom-DBR mirrors. The first low index layer below the cavity was partially oxidized, the aperture shape is parametrized as a square–circle transition with a cylindricity of 0.5 (Fig. 1(b)). The detailed description can be found in Table 3. In Fig. 2, the calculated blueshift of the modes versus the aperture diameter can be seen. Both the predicted mode splitting and the absolute wavelength values show reasonable agreement with the experimental data (Fig. 3), which was measured according to the configuration shown in Fig. 4. A VCSEL wafer of 20 nm × 30 nm was placed on the target holder, and the laser output of a single diode was coupled into a graded-index multi-mode fiber of 50 μm core diameter with the

Table 3
The structure of the simulated VCSEL

Periods	Type	Thickness (nm)	Index
18	$Al_{0.2}Ga_{0.8}As$	60.9	3.492
	$Al_{0.9}Ga_{0.1}As$	69.4	3.065
1	Cavity	244.4	3.482
1	$Al_{0.9}Ga_{0.1}As$	46.3	3.065
	$AlAs/Al_2O_3$	23.6	3.002/1.7
	$Al_{0.2}Ga_{0.8}As$	60.9	3.492
24	$Al_{0.9}Ga_{0.1}As$	69.4	3.065
	$Al_{0.2}Ga_{0.8}As$	60.9	3.492

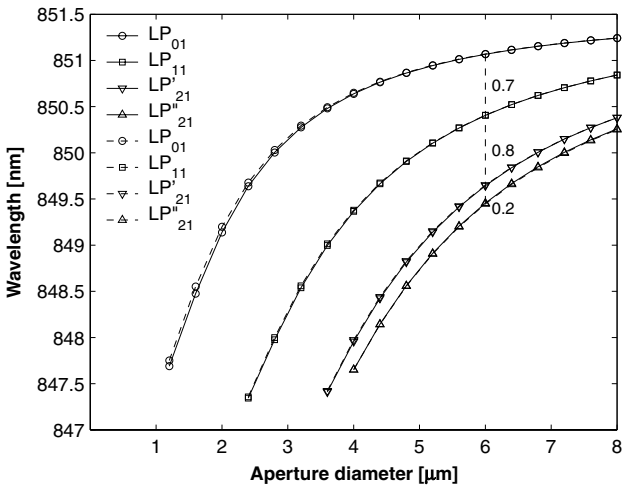

Fig. 2. Calculated wavelength versus aperture diameter. Hybrid WIM results are drawn with continuous, effective radius-WIM results with dashed lines.

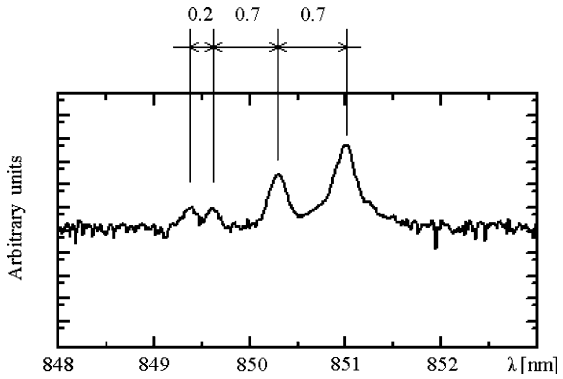

Fig. 3. Experimental emission spectrum.

help of two lenses and a mirror. An Ando AQ-6315 spectrum analyzer with 0.05 nm resolution, connected to a PC, was used to record the spectrum. The environmental temperature was fixed on room temperature, while the VCSEL was driven by a current of 4.5 mA. The redshift of the modal wavelengths due to the slightly increased cavity temperature was calibrated by changing the refractive indices of all layers according to an empirical formula compared to their background values. The wavelength split between the two LP_{21} modes is a direct consequence of the different lateral wavenumbers (k_is in Eq. 12), as the mode

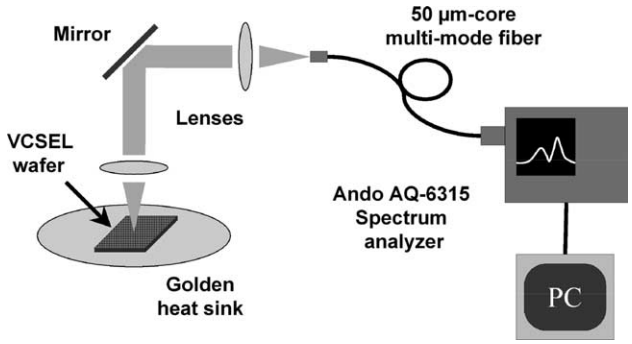

Fig. 4. Setup to record the spectrum.

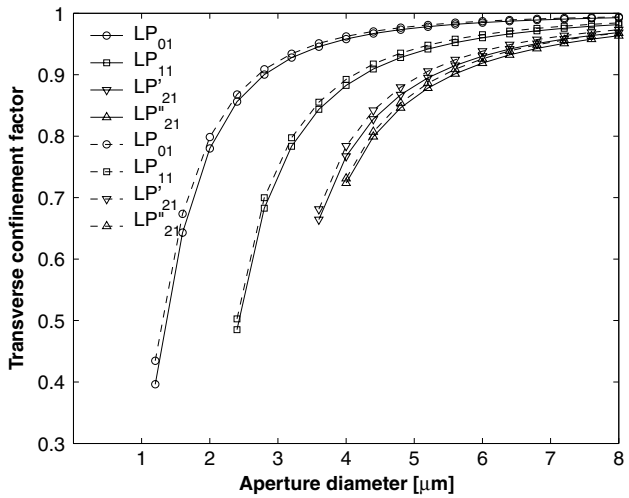

Fig. 5. Confinement factor versus aperture diameter.

with shorter wavelength experiences a shorter effective radius according to its lateral intensity distribution. The mode splitting decreases as the cylindricity parameter increases, finally vanishing in case of the perfect circular aperture.

The dependence of transverse confinement factor on the aperture size is plotted in Fig. 5. A small difference between the cutoff aperture diameters of the two LP_{21} modes also appears. The results of the two methods are nearly the same, near cutoff a difference of 5–10% can be observed between the calculated confinement factors for each mode. In Fig. 6, the intensity pattern of the fundamental and some higher order modes can be seen. They were calculated by the lateral part of hybrid WIM with FDM. As previously predicted, the first higher order mode, LP_{11}, has remained degenerated, the degeneracy of LP_{21} has been splitted (with effective radii of 92% and 87% of r_0, respectively), and LP_{31} is degenerated again. It is important to note that all linear combinations of two degenerated modes are appropriate solutions as well; and since degenerated modes can be seen together distorted ring-like near fields can be observed. However, if the higher order degenerated LP_{21} modes come into play while increasing the current, LP'_{21} will significantly dominate over LP''_{21}, which can be clearly realized on experimental near field patterns.

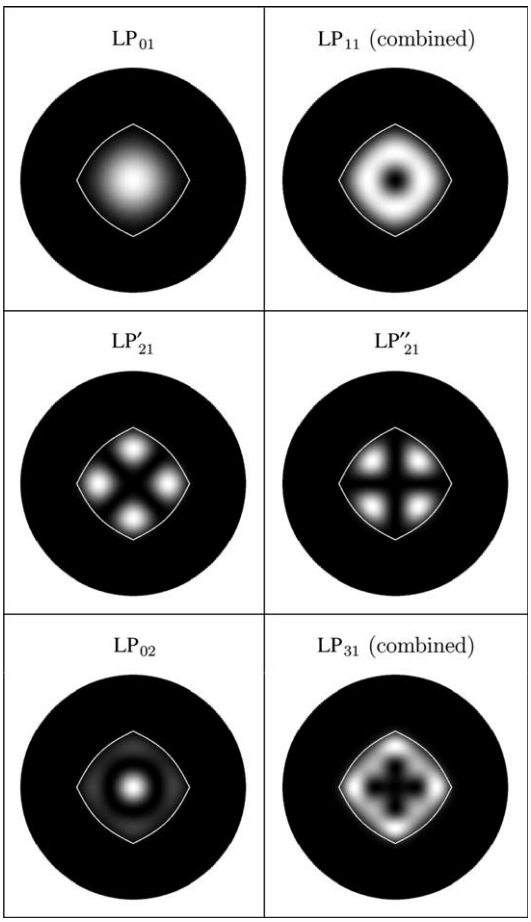

Fig. 6. Mode patterns calculated with FDM. The aperture shape is indicated with white curve.

4. Conclusion

Two methods have been presented in order to calculate the degeneracy splitting and important optical parameters for non-circular apertures. These models do not aim to implement the most accurate and exact full 3-D technique, but to find a compromise between reliable optical data and relatively short simulation time. Both of them have their level in the hierarchical modeling concept. The effective radius-WIM is an intuitive extension of circular WIM, and can be very easily joined to the original algorithm from computational point of view. The proposed scalar hybrid WIM demands to solve a different problem, but has a stronger physical basis. Although both methods neglect the diffraction loss (which may have a significant effect in case of small apertures), they can be extended with an estimation based on the Fresnel-approximation. A natural future improvement can be the vectorial hybrid WIM, in which the same separation is made for both the electric and magnetic fields, but they are coupled at the core-cladding boundaries, and this leads to more complex system matrix.

References

[1] B.J. Thibeault, K. Bertilsson, E.R. Hegblom, E.M. Strzelecka, P.D. Floyd, R. Naone, L.A. Coldren, IEEE Photon. Technol. Lett. 9 (1997) 11.
[2] K.L. Lear, A. Mar, K.D. Choquette, S.P. Kilcoyne, R.P. Schneider, K.M. Geib, Electron. Lett. 32 (1996) 457.

[3] C. Degen, I. Fischer, W. Elsäßer, L. Fratta, P. Debernardi, G.P. Bava, M. Brunner, R. Hövel, M. Moser, K. Gulden, Phys. Rev. A 63 (2001) 23 817.
[4] A. Valle, K.A. Shore, L. Pesquera, J. Lightwave Technol. 14 (1996) 2062.
[5] C. Degen, B. Krauskopf, G. Jennemann, I. Fischer, W. Elsäßer, J. Opt. B: Quantum Semiclass. Opt. 2 (2000) 517.
[6] G.P. Bava, P. Debernardi, L. Fratta, Phys. Rev. A 63 (2001) 23 816.
[7] P. Bienstman, R. Baets, J. Vukusic, A. Larsson, M.J. Noble, M. Brunner, K. Gulden, P. Debernardi, L. Fratta, G.P. Bava, H. Wenzel, B. Klein, O. Conradi, R. Pregla, S.A. Riyopoulos, J.-F.P. Seurin, S.L. Chuang, IEEE J. Quantum Electron. 37 (2001) 1618.
[8] G.R. Hadley, Opt. Lett. 20 (1995) 1483.
[9] G.R. Hadley, K.L. Lear, M.E. Warren, K.D. Choquette, J.W. Scott, S.W. Corzine, IEEE J. Quantum Electron. 32 (1996) 607.
[10] M.J. Noble, J.P. Loehr, J.A. Lott, IEEE J. Quantum Electron. 34 (1998) 1890.
[11] M.J. Robertson, P.C. Kendall, S. Ritchie, P.W.A. McIlroy, M.J. Adams, J. Lightwave Technol. 7 (1989) 2105.
[12] E.R. Hegblom, D.I. Babic, B.J. Thibeault, L.A. Coldren, IEEE J. Sel. Top. Quantum Electron. 3 (1997) 379.
[13] B.E.A. Saleh, M.C. Teich, Fundamentals of Photonics, John Wiley & Sons, New York, 1991.
[14] A. Witzig, Modeling the Optical Processes in Semiconductor Lasers, Hartung-Gorre Verlag, Konstanz, Germany, 2002.
[15] M. Streiff, A. Witzig, W. Fichtner, IEE Proc.-Optoelectron. 149 (2002) 166.
[16] K.L. Lear, K.D. Choquette, R.P. Schneider Jr., S.P. Kilcoyne, Appl. Phys. Lett. 66 (1995) 2616.
[17] T. Rössler, R.A. Indik, G.K. Harkness, J.V. Moloney, C.Z. Ning, Phys. Rev. A 58 (1998) 3279.
[18] R.L. Carter, Molecular Symmetry and Group Theory, John Wiley & Sons, New York, 1998.
[19] J.K. Guenter, J.A. Tatum, R.A. Hawthorne III, B.M. Hawkins, D.T. Mathes, Proc. SPIE 5364 (2004) 34.
[20] P. Debernardi, G.P. Bava, C. Degen, I. Fischer, W. Elsäßer, IEEE J. Quantum Electron. 38 (2002) 73.
[21] M.J. Noble, J.-H. Shin, K.D. Choquette, J.P. Loehr, J.A. Lott, Y.-H. Lee, IEEE Photon. Technol. Lett. 10 (1998) 475.